A Smartphone-Based Method for Assessing Tomato Nutrient Status through Trichome Density Measurement

SHO UEDA.[1], and XUJUN YE[2]
[1]United Graduate School of Agricultural Sciences, Iwate University, Morioka, Iwate, 020-8550, Japan.
[2]Faculty of Agriculture and Life Science, Hirosaki University, Hirosaki, Aomori, 036-8560, Japan

Corresponding author: Sho Ueda.

ABSTRACT Accurately assessing tomato plant nutrient status is crucial for maintaining high yields. Consequently, accurately identifying fertilizer-induced stress through the morphological traits of tomato plants has become a critical agricultural challenge. Research and development efforts have focused on developing noninvasive diagnostic tools for nutrition that leverage a combination of morphological traits and advanced sensor technologies. Given these advancements, detecting fertilizer stress by observing morphological traits near the growth points of tomatoes is still a significant challenge. To address this challenge, we developed a simple and cost-effective smartphone-based method for measuring trichome density. This method involves transferring trichomes from the surface of a leaf onto cellophane tape and capturing images using a smartphone. The images are processed using computer vision techniques to calculate the trichome density. To assess the efficacy of this method, we performed experiments on hydroponically grown tomato plants subjected to varying fertilizer concentrations. Our results indicate that our novel method for measuring trichome density accurately reflects fertilizer stress in tomato plants. The predictive performance of our model, as evaluated by the mean area under the precision–recall curve, was 0.824, despite variations in the measurement data caused by differences in optical conditions. This study introduces an innovative approach for designing diagnostic devices for detecting fertilizer stress in plants by considering the surface structures of plants. Our proposed method represents a straightforward, efficient, and economical approach for evaluating the nutrient status of tomato plants and has the potential to overcome the limitations of conventional noncontact optical methods.

INDEX TERMS Tomato, tomato leaf, fertilizer stress, trichome, smartphone, computer vision, machine learning, precision agriculture

I. INTRODUCTION

Tomato (*Solanum lycopersicum*), a vegetable that is widely cultivated worldwide, is influenced by various environmental factors that affect its production and quality.

The nutrient status of plants, one of the most crucial factors influencing tomato yield, is an important consideration in tomato production. Therefore, accurately assessing plant nutrient status is essential for maintaining high tomato yields.

Techniques have been developed to analyze the constituents of fertilizers in soil, media, and nutrient solutions, aiming to estimate the amount of nutrients absorbed by plants [1],[2]. Additionally, researchers have developed invasive methods to analyze plant nutrients [3],[4]. Moreover, noninvasive techniques such as visual inspection and sensor-based monitoring are available for assessing plant traits.

Morphological changes serve as crucial indicators for nutrient analysis, particularly in the context of environmental stressors such as drought and nutrient deficiency [5],[6],[7]. This approach is equally relevant for crops cultivated under controlled, artificial conditions. These changes manifest in the patterns of vegetative and reproductive growth observed in plants [8],[9]. The ability to detect and examine these modifications allows for a more sophisticated understanding of the nutrient levels of plants and their responses to varying environmental conditions.

Leaf area and chlorophyll content, which are related to leaf color and spectrum, are commonly used as indicators of the adaptive response of plants to fertilizer stress

[7],[10],[11],[12],[13],[14]. These methods have led to the development of a diagnostic framework based on the relationships among fertilizer application, phenotypic expression, and yield outcomes. Analyzing the colors and spectral data of plant canopies enables predictions of plant health and productivity. These predictions utilize wide-area imagery from satellites, aircraft, and drones combined with data collected from in-field sampling stations. The aforementioned optical observation techniques, which utilize reflected light from the plant body, effectively address the need for noninvasive and rapid monitoring of phenotypes [7]. Furthermore, this technique has been investigated in tomato leaves.

II. RELATED WORK

To promptly identify morphological alterations resulting from environmental influences, it is preferable to assess the canopy close to the growing points associated with plant cell differentiation. Nevertheless, there is a notable lack of studies in the literature identifying the phenomenon of fertilizer stress, especially in relation to the assessment of young tomato leaves. Gianquinto et al. conducted a study using a multispectral radiometer positioned directly above the tomato plant canopy to investigate the correlation between light reflectance, chlorophyll concentration, and total Kjeldahl nitrogen content in an intervention study of fertilizer application. By employing this noncontact arrangement, measurements were conducted without physically interacting with the leaves. They discovered a linear relationship between optical reflectance and chlorophyll concentration; however, no such linear relationship was identified between optical reflectance and total Kjeldahl nitrogen content [11]. Similarly, Padilla et al. directly observed the most recently fully expanded leaves using an optical chlorophyll meter (Konica Minolta, SPAD-502), revealing a linear relationship between optical observations and the nitrogen nutrition index under conditions of flattened leaf surface structure [12]. In both investigations, it is assumed that there is an absence of any barriers along the path of light between the observing device and the plant leaves, highlighting a gap between the specifications of diagnostic equipment for farmers and the current state of research and development.

However, in contrast to other crops, tomatoes have an abundant number of trichomes—small projections or hair-like structures—on the surface of their leaves (Figure 1). Trichomes are densely concentrated on young, actively growing leaves and sparsely distributed on older leaves [15]. The presence of surface microstructures on plant bodies, such as trichomes, is known to significantly affect their appearance [16],[17],[18]. Given the high density of trichomes on young tomato leaves, it is plausible that trichomes may influence the effectiveness of optical sensing techniques used to assess the nutrient status of tomato plants. Consequently, the presence of trichomes

should be considered a potential practical limitation when using optical sensing techniques on young tomato leaves to evaluate fertilizer stress. However, current methodologies do not adequately address the impact of trichomes on optical sensing techniques used for the rapid assessment of tomato plant nutrient status.

FIGURE 1. Abundant number of trichomes—small projections or hair-like structures—on the surface of tomato leaves.

Counting trichomes, which are abundant on young tomato leaves, is not easily achievable by visual means. Manually counting trichomes using a microscope is one of the few available methods for quantifying their density, as trichomes are abundant on young tomato leaves and not easily distinguishable by visual means alone. The lack of a specialized device for assessing trichome density may have hindered progress in this area of research.

Chlorophyll content, which is correlated with leaf color, is a widely used indicator of fertilizer stress in plants. However, it is not the only marker. Trichomes have also been identified as potential indicators of fertilizer stress, as they contribute to plant defense against pests by responding to fertilizer stress and altering plant density [19],[20]. Various types of trichomes can be observed on the surface of tomato leaves, the majority of which are short, hair-like trichomes and trichomes with large, spherical cells at their tips (known as Type VI trichomes, Figure 2) [21]. The glandular head of Type VI trichomes is connected to the stalk cell at the base by fragile cell walls [22].


FIGURE 2. Type VI trichomes on the tomato plant surface.

This structural arrangement allows the glandular part to easily detach from the leaf surface upon physical stimulation, and the mucilage within the glandular part is known to inhibit pest activity.

Researchers have observed multiple instances where trichomes respond to fertilizer stress [19],[20],[23]. For

example, Barbour et al.'s investigation revealed an inverse relationship between fertilizer application, leaf nitrogen content, and trichome density [19]. Similarly, Hoffland et al. reported a positive correlation between the leaf carbon-to-nitrogen ratio and trichome density [20]. In contrast, Leite et al. presented data indicating that trichome density increased over time when less fertilizer was used compared to that of conventional farming methods [24]. Despite these findings, the majority of previous studies have focused on investigating trichome density within a biological context, with limited exploration of techniques to observe trichome density in agricultural production settings without advanced laboratory equipment, highlighting the need for further research to develop practical methods for assessing trichome density in real-world agricultural environments.

To address this gap, the present study focuses on tomato leaf trichomes and explores their potential as indicators for assessing the nutrient status of tomato plants. As depicted in Figure 3, our main hypothesis is that leaf trichome density is influenced by fertilizer level, suggesting its potential as an additional indicator of plant nutrient status in conjunction with traditional fertilizer stress markers such as leaf nitrate content. This conceptual framework serves as the foundation for our data-driven analysis. To achieve this goal, it is necessary to develop a tool for assessing trichome density. The identification of distinct items within a particular setting containing several objects inside the visual field is commonly regarded as a computer vision problem [25],[26]. Given this context, we hypothesized that utilizing cameras could convert the challenge of measuring trichome density to a problem analogous to an object detection problem.
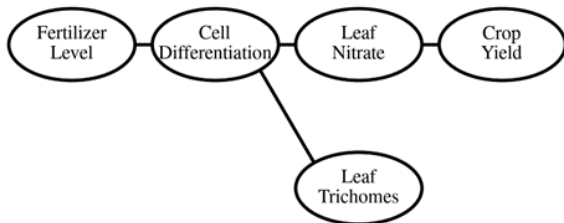
FIGURE 3.Hypothesized relationships between fertilizer level, cell differentiation, leaf nitrate content, number of leaf trichomes, and crop yield for tomato plants, serving as the conceptual framework for the study.

In recent years, the growing popularity of smartphones has driven the advancement of proof-of-concept agricultural technologies that harness their advanced computational capabilities, high-resolution cameras, and internet access [27],[28],[29],[31]. Building on this trend, we aimed to investigate the feasibility of using smartphones as a cost-effective tool for measuring trichome density, which can serve as a predictive indicator of tomato plant nutrient status.

III. MATERIALS AND METHODS

A. Development of a Smartphone-Based Trichome Density Measurement Method

1) Design of a Simple Kit for Collecting Trichomes from Tomato Leaves

In this study, we designed a straightforward kit to measure the density of Type VI glandular trichomes on tomato leaves. The kit consists of custom-made measurement paper crafted from inkjet-printable cardstock and cellophane tape (NICHIBAN, CT-18), enabling cost-effective measurements (Figure 4). This paper contains augmented reality (AR) markers, enabling the distance of objects within captured images to be precisely measured. Additionally, there is a 12 mm × 12 mm opening in the center of the paper. A piece of cellophane tape is affixed to the back of the paper, covering this opening. This tape is used to extract trichomes that are present on the surface of tomato leaves.

FIGURE 4.A smartphone was used to capture an image of the diagnostic kit.

Optimizing a technique that involves the use of cellophane tape for trichome extraction allows the creation of a highly cost-efficient kit. Although recent advances in sophisticated object detection algorithms utilize complex neural networks, they typically demand high-speed parallel processing, significantly increasing computational costs. Our approach, which utilizes cellophane tape for trichome extraction, circumvents the need for such intensive computational resources and enables the use of less computationally demanding algorithms for trichome detection. Thus, this approach reduces the overall cost of the assessment process, making it more economically viable.

The purpose of this diagnostic kit is to meet the technological progress needs in agricultural production areas that lack access to laboratory-level experimental facilities. Therefore, to minimize the number of components required for measurement, the kit is specifically designed to allow for

dual manual operation. The measuring paper is held by one hand, while the smartphone is operated by the other hand (Figure 4). The statistical model accounts for the variability in the results caused by varying optical conditions for each shot. The kit is designed to prioritize user friendliness as a minimum viable product in lean startup methodology for manufacturing and software development, enabling the measurement of trichome density without requiring technical expertise [32]. The practical application of this technology in the field is well suited due to its simplicity and cost-effectiveness (Figure 5).
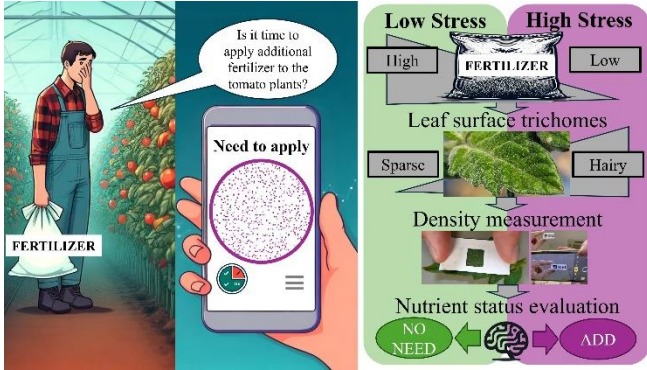

FIGURE 5. Proposed concept of the tomato cultivation support framework.

2) Trichome Transfer and Image Capture

To acquire images, the kit is used to transfer trichomes from tomato leaves onto cellophane tape. Subsequently, a smartphone is used to capture an image of the measurement paper with the transferred trichomes. This captured image is then processed and analyzed to calculate the trichome density, which serves as an indicator of the abundance of trichomes on tomato leaves.

3) Image Processing Pipeline

The image processing process involves several steps. The process begins with preprocessing the obtained images, and then features are extracted from these images. Specifically, the preprocessing steps include reading the metadata (exchangeable image file format (EXIF)) embedded in the image files, identifying the augmented reality (AR) markers within the images, applying homography transformations to align the images, and adjusting variations in the lighting conditions. For feature extraction, we focused on identifying trichomes in images. We leveraged the unique shape and structure of Type VI glandular trichomes and applied binarization and noise removal filtering algorithms. Additionally, we utilized AR markers to convert pixel counts in each image to relative distances, allowing for accurate trichome distance estimation. Finally, we calculated the

trichome density for images captured under various environmental conditions and camera settings, each containing distinct EXIF data. Figure 6 shows the flowchart detailing how we computed trichome density from the images obtained with the trichome measurement kit we developed. The image processing described above was carried out using the software specifications listed in Table 1.

a)   EXIF Data Reading

Images contain metadata, specifically EXIF data, which provide information about the environmental conditions during image capture and the camera settings. In this study, we analyzed EXIF data to gain insights into the environmental conditions and camera settings used during image capture.

b)   AR Marker Detection

AR markers were used to determine the absolute scale and orientation of the image, allowing object distances to be calculated. AR markers were detected using the ArUco module of the OpenCV library [33]. The specific AR marker dictionary used was DICT_4X4_250 from the ArUco library.

c)   Homography Transformation

Homography transformation was utilized to correct perspective distortion in images caused by positional and orientational variations of the measurement paper relative to each camera capture, adjusting the images as though the camera and the measurement paper were parallel. This process involves using the coordinates of the four corners of a region on the measurement paper, obtained from detecting AR markers, as reference points to estimate a perspective transformation matrix. The "warpPerspective" function of the OpenCV library was employed for this task.

d)   Illumination Correction

Illumination correction involves compensating for nonuniform lighting using flat field correction [34]. The correction process is described by Equation (1), where C represents the corrected image obtained by multiplying the precorrection image R by the average luminance m and dividing it by the smoothed image F. To apply the smoothing filter, we utilized the "blur" function from the OpenCV library. Before performing illumination correction, all images were resized to dimensions of 1000 pixel × 1000 pixel, and a 50 pixel × 50 pixel averaging filter was applied.
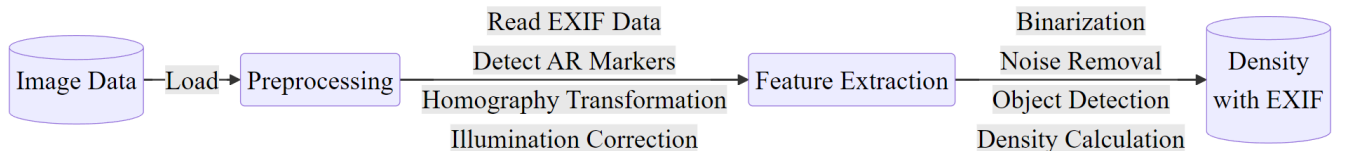
$$C = \frac{R \times m}{F} \tag{1}$$

FIGURE 6. Flow of image analysis from data acquisition to feature extraction.
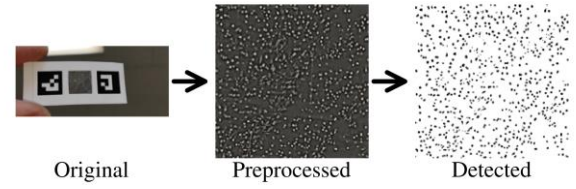
$$p = p_1, p_2, \cdots, p_n \qquad (2)$$

4) Feature Extraction

a) Noise Removal

The "morphologyEx" function of the OpenCV library was utilized for noise removal. This function was used to perform an opening operation, which is a morphological transformation that removes small-scale noise from the image while preserving the overall shape of the objects of interest.

b) Object Detection

The "watershed" function of the OpenCV library was used for segmentation, identifying boundary surfaces that separate contours in the image and enabling the recognition of individual trichomes. During this procedure, we identified individual trichomes on the adhesive surface of the cellophane tape. Type VI trichomes are characterized by their spherical heads [35], fragile layer aiding head detachment [22], and relatively large average diameter of approximately 60 µm [22] compared to other trichomes. We distinguished Type VI glandular trichomes using physical and optical filtering based on specific properties. The identification of trichomes is based on the assumption that a substantial quantity of glandular trichomes exist on the leaf surface, as previously mentioned.

In this paper, we utilize the term "trichomes" to describe the contours of detected objects based on the following criteria:

- A detachable layer must exist, allowing for peeling using cellophane tape;
- The object should be larger than a pixel, with a minimum size of approximately 10 µm, and must be detectable in the image;
- The lower limit of the shape factor within the survey area is defined as the 1st quartile minus 1.5 times the interquartile range;
- The upper limit of the shape factor within the survey area is defined as the 3rd quartile plus 1.5 times the interquartile range;
- The object's shape should more closely resemble a sphere than an elongated hair-like shape, with the circularity exceeding a defined lower limit;
- The perimeter of the object falls within a specified range, defined by a lower and upper limit;
- The area of the object lies within a specified range, defined by a lower and upper limit;

The contours detected through segmentation yield centroid points, denoted as p in Equation (2). These points exist within a two-dimensional space and are represented using the pixel coordinates of the image. Figure 7 shows the image processing steps performed up to this point, including preprocessing and object detection.

FIGURE 7.Example of image data preprocessing and object detection.

5) Density Calculations

The density was computed for the centroid points denoted as p in Equation (2). The nearest neighbor distance (NND), calculated using Equation (3) [36], was determined by measuring the distance between the nearest neighboring points within a given set. The NND algorithm utilizes the Euclidean distance, represented as $d(p, q)$, which measures the distance between a point p and its closest point q. This value is then averaged over the total number of contours n present in the image. The computation of $d(p, q)$ was performed using a k-dimensional tree algorithm implemented through the "Nearest Neighbors" class from the neighbors module of the scikit-learn library [37], [38].

$$NND = \frac{1}{n} \sum_{i=1}^{n} d(p, q) \qquad (3)$$

A higher NND value indicates a sparser arrangement of contours, while a lower value suggests denser groupings. Notably, glandular Type VI trichomes may become detached from the leaf surface due to factors such as insect infestations or physical abrasion. However, the NND is less sensitive to these factors than is a density index that relies on the object count per unit area, as the NND represents density as a probability distribution. As a result, even if some areas of the image are affected by trichome detachment, the NND can still provide a reliable density estimate as long as unaffected regions remain.

B. Evaluation of the New Method for Assessing the Nutrient Status of Tomato Plants

1) Tomato Growth Conditions in Hydroponic Culture for Fertilizer Stress Experiments

The tomato cultivar (TAKII SEED, Fruitica) was grown hydroponically using the deep water culture (DWC) in a greenhouse at Hirosaki University, Japan, with natural light as the sole source of illumination. The DWC is a hydroponic method in which plant roots are completely submerged in a nutrient solution within a production tank [39], [40]. Applying this cultivation technique avoids a variety of impediments arising from the soil, thereby facilitating the growth of tomatoes without water stress. In this study, 15-liter plastic buckets were used, with a planting density of 8 plants per 180 cm × 90 cm bed. The buckets were equipped with lids containing center holes for the tomato stems to prevent algae growth in the nutrient solution.

Within these buckets, the nutrient solution was aerated and mixed by introducing air. The air was supplied by a blower

(YASUNAGA, AP-40P) and divided into eight segments.

Each segment was channelled through silicone tubing and dispersed into the nutrient solution using air stones to ensure proper mixing and oxygenation. The nutrient solution, which was prepared using a hydroponic fertilizer (OAT Agrio, Fertilizer Series SA), was maintained at three different total dissolved solids (TDS) concentrations: high (1500 ppm), medium (1000 ppm), and low (500 ppm).

The fertilizer plots were arranged in a randomized block design, as depicted in Figure 8. In the preliminary experiment, tomato plants were grown in the empty spaces indicated in Figure 8. Water was added to the buckets as needed when the nutrient solution concentration decreased. Fertilizer was applied every two weeks, and nutrient solution concentrations were adjusted to maintain the desired TDS levels, which were measured using a TDS meter (EUTECH, PCSTestr35). The fertilizer used in the experiments closely matched the nutrient uptake ratios of the tomatoes, enabling the utilization of closed hydroponic systems without the need for nutrient solution replacement [41]. However, during the cultivation period, the system was not maintained as a completely closed system; nutrient solutions were replaced whenever they became cloudy due to the presence of algae or root debris.

During the cultivation period, before the compound leaves were harvested, two plants were lost. As a result, 20 plants remained available for inclusion in the study. Furthermore, an additional two plants were lost by the end of the fruit harvesting period, resulting in 18 plants being available for harvest yield assessment.
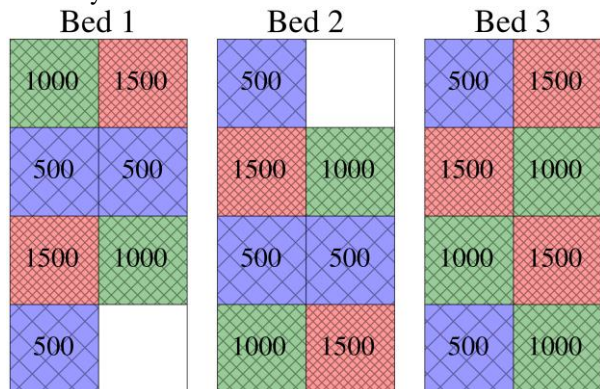

FIGURE 8. Experimental layout with three different fertilizer levels (ppm) in a randomized block design.

2) Compound Leaf Sampling and Trichome Transfer

The experiment involved collecting compound leaves. A total of 40 compound leaf samples were collected during two separate harvesting sessions in March and April 2023. The compound leaves were sampled 15 cm below the apical meristem. For trichome density measurements, we selected all leaflets larger than the opening of the measurement paper (12 mm × 12 mm) from each compound leaf to ensure a consistent sampling area. We used the same number of measurement papers as the number of leaflets, ensuring an accurate assessment of trichome density distribution on each leaflet. Before the smartphone images were captured, the glandular trichomes were transferred from the leaflet surface to the measurement paper. The leaflets were affixed to the adhesive side of the cellophane tape (Figure 9), and each leaflet was gently pressed with a finger to ensure complete contact between the leaf surface and the tape. After removing the leaflet, the cellophane tape with the transferred trichomes was photographed alongside the measurement paper.
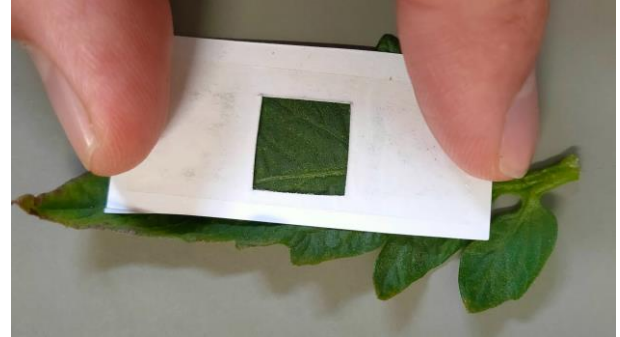
FIGURE 9. Trichome transfer process from the leaflet surface to the measurement paper using cellophane tape.

3) Image Acquisition and Dataset Preparation

The measurement paper was photographed using the native camera app on a smartphone (OPPO, Reno A). The camera mode was set to automatically adjust the exposure, ISO sensitivity, and focus. Additionally, the smartphone's built-in white LED was activated for auxiliary lighting, and the measurement paper was illuminated by oblique light from the ceiling's fluorescent lighting (as shown in Figure 4). To account for potential bias caused by varying optical conditions during the analysis stage, multiple images were captured by adjusting the positions and angles of the camera and measurement paper, thus creating a range of lighting conditions. The image composition was carefully designed to ensure that the measurement paper was positioned in the middle, facilitating the identification of the AR markers. Immediately after the images were captured, a preliminary analysis was conducted to verify the completeness of the image processing pipeline. All the measurement papers were checked to ensure that they could be included in the dataset. In cases where the analysis program encountered exceptions, rephotography was performed to prevent bias due to missing information from the measurement paper during analysis. Consequently, this study focused exclusively on calculating trichome density from images where AR markers could be detected. It was assumed that the accuracy of AR marker detection would not impact the results. This assumption was based on the practical consideration that the detection accuracy of AR markers and other 2D codes is primarily dependent on the library used and has already reached a practical level for real-world applications. Moreover, in the event of an error, the user of the kit can rectify the problem by performing rephotography. After the data collection and preprocessing steps, information from all the measurement papers was included in the final dataset, which consisted of

6,855 images suitable for analysis.

4) Nitrate Concentration Measurement in Tomato Leaves

After measuring trichome density, the tomato leaves were frozen using a refrigerant (HFO-1234ze) to facilitate cell wall structure breakdown and juice extraction. The leaves were placed in zippered plastic bags before freezing, allowing for the escape of moist air caused by refrigerant evaporation and preventing moisture accumulation within the bags. The frozen leaf samples were then thawed and mechanically pressed using pliers to extract the leaf juice. The extracted leaf juice was stored at -20 °C for further analysis. After storage, the leaf juice was thawed and centrifuged to separate the solid and liquid components. After centrifugation, the clear supernatant was carefully collected, ensuring that no sediment particles were transferred. Electrophoresis buffer (Otsuka Electronics, α-AFQ133) was used to dilute the leaf juice 20–40 times. The diluted leaf juice was then filtered through a 0.45 µm pore size syringe filter. The nitrate ion concentration in the filtered solution was measured using a capillary electrophoresis system (Agilent Technologies, 7100). A capillary tube with an internal diameter of 75 µm and a length of 72 cm was utilized. The experimental parameters were as follows: buffer temperature, 25 °C; voltage, 20 kV; injection time, 4 seconds; injection pressure, 50 mbar; and detection wavelength, 350 nm. The nitrate ion concentration was determined using the absolute calibration method, where the measurements were based on a standard sample with a known concentration. The nitrate ion concentration was measured once for each compound leaf, yielding a total of 40 scalar values. The nitrate ion concentration measurements were then combined with the trichome density measurements obtained from 6,855 images to create the dataset (Figure 10). This dataset was used for further analysis using a data-driven approach.
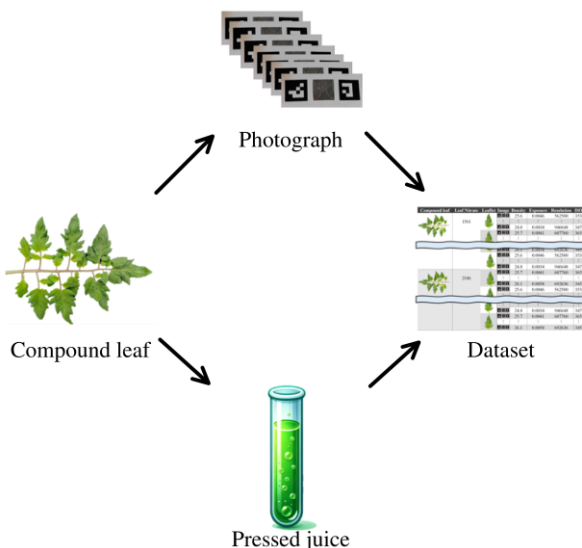

FIGURE 10.Workflow from data acquisition to analysis.

5) Assessment of Tomato Fruit Harvest Under Experimental Conditions

The fruit yield of the tomato plants was evaluated under experimental conditions. All fully ripened red fruits were harvested from each plant. After harvesting, the fruits were stored at 5 °C and subsequently weighed.

C.   Data Analysis

1) Configuration of the Data Analysis Environment

The analytic environment was built using Docker [42], a technology for operating system-level virtualization. Docker is a tool for reproducing the same working environment across different computer systems, ensuring consistency and reproducibility of analytical results, regardless of the computer's specifications. The analysis was conducted using Python [43] version 3.10 with the Docker image jupyter/datascience-notebook [44]. Table 1 provides a comprehensive list of the Python library versions and Docker image versions utilized in this study. The opencv-contrib-python, imbalanced-learn [45], lightgbm [46], shap [47], and ExifRead [48] libraries were utilized for image processing, dataset preprocessing, machine learning model training, model interpretation, and metadata extraction from image data, respectively.

TABLE I
VERSIONS OF LIBRARIES AND DOCKER IMAGE USED

Library/Image	Version
jupyter/datascience-notebook	cde8b4389ade
opencv-contrib-python	4.6.0.66
imbalanced-learn	0.12.0
lightgbm	3.3.5
shap	0.43.0
ExifRead	3.0.0

2) Multicollinearity and Variable Interaction Assessment

Before building the model, we investigated the potential presence of multicollinearity and interaction effects among the predictor variables. Multicollinearity occurs when there is a strong intercorrelation between predictor variables, which can result in unstable and unreliable regression coefficient estimates. To detect the presence of multicollinearity, we utilized the variance inflation factor (VIF), which measures the extent to which the variance of a regression coefficient estimate increases due to the correlation among predictor variables. A VIF value surpassing the cutoff point of 10 is commonly considered a strong indication of problematic multicollinearity [49]. In an effort to enhance the model's interpretability and alleviate the consequences of multicollinearity, we removed variables with VIF values surpassing the threshold of 10 from further analyses.

Moreover, we explored the possibility of interaction effects among the predictor variables, which arise when the impact of one predictor variable on the response variable is influenced by the level of another predictor variable. To uncover potential interactions between features, we

conducted a stratified analysis involving dividing the data into subgroups based on the levels of a suspected interacting variable and assessing the relationship between the predictor and response variables within each subgroup. Specifically, we investigated how image resolution might modulate the association between trichome density and nitrate concentration in tomato leaves.

3) Predicting Tomato Fertilization Requirements Based on Leaf Trichome Density

The primary objective of this study was to develop a kit that is suitable for practical use in the field. By leveraging existing knowledge on the correlation between leaf nitrogen-related indicators, which are affected by various levels of fertilizer stress, and trichome density, we aimed to address a crucial question for farmers: is there time to apply additional fertilization to tomato plants in the field? Consequently, we formulated a binary classification problem to determine the need for fertilization based on leaf nitrate ion concentrations. The threshold for the leaf nitrate ion concentration was set as a parameter in the model and used to determine whether additional fertilization was necessary. To evaluate the model's generalization performance, leave-one-out cross-validation (LOOCV) was conducted for each compound leaf. The predictive performance of the model was assessed by inputting 1-25 images per compound leaf into the model and evaluating its performance for each case. Figure 11 presents a schematic overview of the data analysis workflow, with the main processes of model training and evaluation described in detail below.
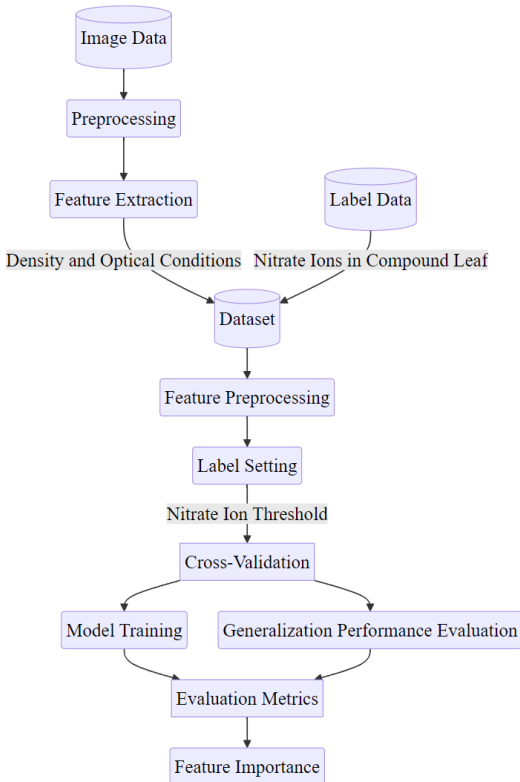

FIGURE 11.Schematic overview of the data analysis workflow.

4) Feature Preprocessing and Label Setting

The objective of the modeling was to determine the need for additional fertilization by comparing the nitrate ion concentration, estimated from trichome density in images, with a predefined threshold. Consequently, leaves were labeled 0 (indicating no need for additional fertilization) or 1 (indicating the need for additional fertilization) based on whether the nitrate ion concentration was below or above the threshold, respectively.

5) Model Training

The dataset was partitioned into training and testing sets before the modeling process. The modeling task involved binary classification, with the data being divided based on each compound leaf. To address the imbalance in both the number of images between compound leaves and leaflets and the class labels, the minority class was oversampled using the synthetic minority oversampling technique (SMOTE) implemented in the imbalanced-learn library [45], [50], [51].

Modeling was performed using a light gradient boosting machine (LightGBM), a decision tree-based approach that employs gradient boosting techniques to combine multiple decision trees for learning purposes [50]. In LightGBM, each decision tree utilizes the residuals from the previous tree to iteratively improve the overall predictive accuracy of the model. The regression predictions z were calculated using Equation (4) [52].

$$z = \sum_{k=1}^{K} f_k(x) \qquad (4)$$

In Equation (4), $f_k(x)$ is defined as the output generated by the k-th decision tree. Here, k represents the total number of decision trees, and x corresponds to the input feature vector. The regression prediction z is then passed through the sigmoid function, as shown in Equation (5), to calculate the probability $\hat{y}$.

$$\hat{y} = \frac{1}{1 + e^{-z}} \qquad (5)$$

The sigmoid function in Equation (5) maps the value of z to a probability between 0 and 1, which is then interpreted as the likelihood of the input belonging to class 1. By applying the sigmoid function to the regression predictions z, as shown in Equation (5), we simulated a scenario in which farmers are provided with the predicted probabilities of nutrient deficiency, enabling them to make informed decisions about the application of additional fertilization to their fields. The final class label $\hat{Y}$ was determined based on the computed probability $\hat{y}$, according to the decision rule outlined in Equation (6).

$$\hat{Y} = \begin{cases} 1 \ if \ \hat{y} \geq 0.5 \\ 0 \ if \ \hat{y} < 0.5 \end{cases} \qquad (6)$$

6) Model Evaluation and Feature Importance

The predicted labels $\hat{Y}$ were compared to the true labels, and performance metrics were computed. The evaluation metric used during training was the area under the precision–recall curve (AUC-PR), as defined by Equation (11). To

evaluate the performance of the trained model on the test data, several evaluation metrics were employed, including the *precision, recall*, F_1, area under the receiver operating characteristic curve (*AUC-ROC*), *AUC-PR*, and mean AUC-PR (*mPR*). These metrics are described by Equations (7)-(12).

The precision, as defined by Equation 7, is the ratio of correctly predicted positive observations to the total number of predicted positives [53],[54].

$$Precision = \frac{True\ Positive}{True\ Positive\ +\ False\ Positive} \quad (7)$$

Equation (8) defines recall as the proportion of accurately predicted positive observations in relation to the total number of true positives. This metric evaluates the model's ability to identify all relevant positive instances.

$$Recall = \frac{True\ Positive}{True\ Positive\ +\ False\ Negative} \quad (8)$$

Equation (9) represents the F_1 score, which is calculated as the harmonic mean of the precision and recall. This metric serves as a balanced measure of both metrics.

$$F_1 = \frac{Precision\ \times\ Recall}{Precision\ +\ Recall} \quad (9)$$

Equation (10) represents the *AUC-ROC*, which is the area under the curve of the true positive rate versus the false-positive rate. The term $t(f)$ denotes the true positive rate at a given false-positive rate f. This measure effectively summarizes the model's ability to discriminate between the positive and negative classes across all possible thresholds, providing a single scalar value that reflects the trade-off between sensitivity (true positive rate) and specificity (1 – false-positive rate).

$$AUC\text{-}ROC = \int_0^1 t(f)\ df \quad (10)$$

Equation (11) represents the *AUC-PR*, which defines the area under the precision versus recall curve. The symbol $p(r)$ represents the precision at a given recall value r. This metric provides a single scalar value that summarizes the trade-off between precision and recall across all possible thresholds. The *AUC-PR* is particularly useful for datasets with imbalanced class distributions, as it provides a more informative measure than does the AUC-ROC [54].

$$AUC\text{-}PR = \int_0^1 p(r)\ dr \quad (11)$$

Equation (12) provides a definition for mPR, which quantifies the AUC-PR for various thresholds k of nitrate ion concentration. To provide a more precise evaluation, the algorithm calculates the average AUC-PR value within the specified threshold range of 1600 to 1900 parts per million (ppm) of nitrate ion concentration. The establishment of this threshold range is based on the concentrations of nitrate ions observed in tomato leaves that have demonstrated favorable yields. In the agricultural domain, it is impractical to consider a situation where a model incorporating a threshold resulting in a decrease in crop productivity would be

employed. For each threshold k, the cumulative AUC-PR$_k$ is divided by the total number of models m. Within this framework, the AUC-PR$_k$ represents the area under the precision–recall curve for a specific threshold k, while m denotes the total number of models considered. The mPR is used to assess the model's performance across a wide range of threshold values, evaluating its effectiveness in various operational scenarios.

$$mPR = \frac{1}{m} \sum_{k=1600}^{1900} AUC\text{-}PR_k \quad (12)$$

To enhance the comprehensibility of the model, we depicted the significance of each feature by utilizing Shapley Additive exPlanations (SHAP) values [55].

IV. RESULTS

A. Nitrate Ion Concentration in Compound Leaves as a Lagging Indicator of Fertilizer Stress

Figure 12 shows the distribution of nitrate ion concentrations in compound leaves 15 cm from the apical meristem in the experimental plots subjected to three different fertilizer concentrations: high, medium, and low. Higher levels of fertilizer application led to a significant increase in the concentration of nitrate ions within the compound leaves. This finding indicates that the nitrate ion concentration in compound leaves can serve as an indicator of fertilizer stress. Nevertheless, the relationship between nitrate ion concentration and fertilizer level is subject to uncertainty. This observation emphasizes the significance of investigating nitrate ion absorption by plants rather than depending exclusively on fertilizer levels as an indicator of fertilizer stress. This approach can account for the inherent uncertainties beyond the scope of fertilizer application rates, particularly those factors that may impede fertilizer absorption.
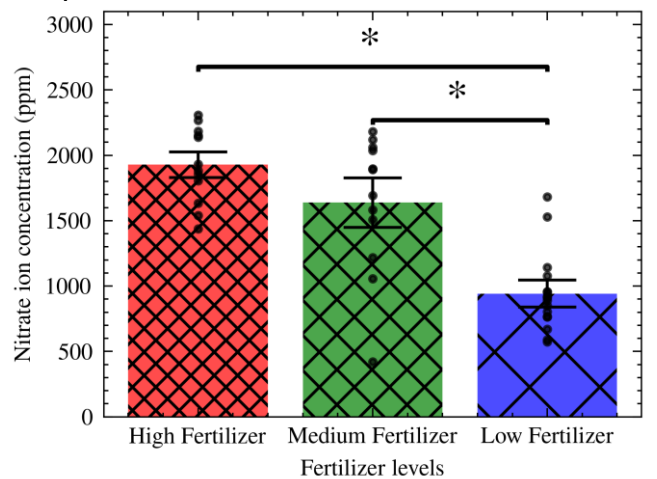

FIGURE 12. Distribution of nitrate concentrations in compound leaves at different fertilizer levels.

B. Leaf Nitrate Concentration as a Leading Indicator of Fruit Yield

Figure 13 shows a positive correlation between fruit yield and nitrate concentration in compound leaves. This finding indicates that the nitrate ion concentration in compound leaves can serve as an indicator of fruit yield. Generally, crop yield tends to increase with increased fertilizer absorption; however, excessive fertilizer application beyond a certain threshold can lead to reduced yields [4],[8],[9]. The findings of this study indicate that fertilizer application in the experimental field fell below this critical threshold, suggesting that the tomatoes experienced stress due to insufficient fertilization. The primary goal of fertilizer application in agriculture is to increase crop yield. Consequently, farmers set specific thresholds based on leaf nitrate concentrations to maintain high yields, applying fertilization when values fall below these thresholds. In this study, the third quartile value of 1,783 ppm derived from the measured leaf nitrate concentrations was used as the threshold for maintaining high yields.
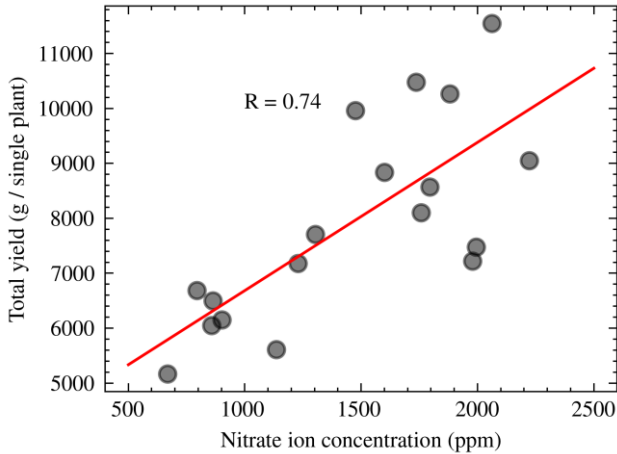

FIGURE 13.Relationship between nitrate ion concentration in compound leaves and yield.

Figure 14 displays the cumulative yield of the experimental setup, obtained through the weighted average of each intervention trial plot within the experimental environment. Considering the planting density, the final fruit production capacity of the experimental apparatus is 39.12 kg/m². This value is not substantially lower than the commercial yields of tomatoes reported in previous studies [56]. Thus, it can be concluded that the environmental conditions in this experimental setup adequately simulated those found in commercial tomato production.
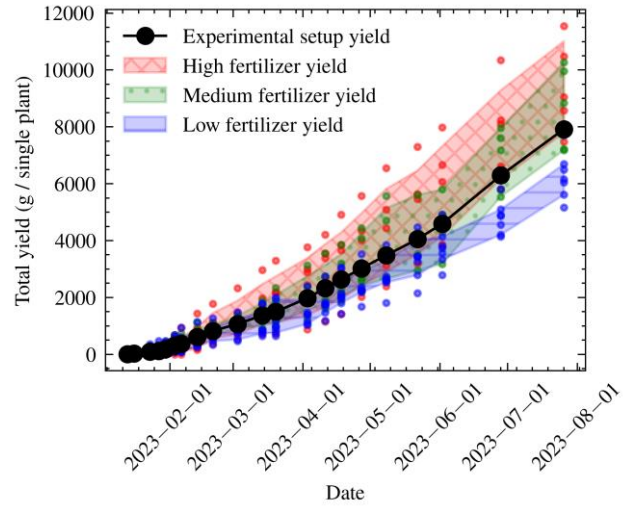

FIGURE 14.Cumulative fruit yield in the experimental setup.

C. Handling of Multicollinearity and Variable Interaction in Data Analysis

Table 2 presents the variance inflation factor (VIF) for each variable. The results reveal an exceptionally high VIF of 47.799 for the ISO speed ratings, which is above the typical threshold of 10, indicating the presence of multicollinearity. This finding suggests that ISO speed ratings are likely influenced by multicollinearity within the dataset. The high VIF value for the ISO speed ratings may be attributed to the camera's automatic adjustment of the exposure time and ISO sensitivity based on the light level detected by the imaging sensor, which effectively regulates image brightness. In the captured images, trichomes appear as white points due to the reflection of light emitted by the smartphone's LED. This reflected light is then detected by the imaging sensor. Consequently, the presence of trichomes influences the image brightness, as the camera adjusts both the exposure time and ISO sensitivity based on the trichome density. Essentially, the results presented in Table 2 indicate that the camera's real-time exposure adjustment algorithm may have led to ISO sensitivity becoming dependent on trichome density, resulting in the observed multicollinearity.

TABLE II
EXAMINATION OF MULTICOLLINEARITY THROUGH THE VIF

Feature	VIF
Nearest Neighbor Distance	43.60
Resolution	11.03
Exposure Time	4.98
ISO Speed Ratings	47.80

The resolution value exhibits interactions and a shift in the intercept, necessitating its inclusion as a variable within the statistical model. An investigation of the effect of resolution on the relationship between trichome density and nitrate concentration in compound leaves reveals varying coefficients and intercepts in the regression equation. These changes in the coefficients with respect to the resolution are demonstrated in Table 3 and Figure 15. The resolution

inherently varies due to factors such as camera performance and the distance between the camera sensor and the measurement paper. As a result, in the dataset used in this study, the resolution acts as an indicator of the distance between the camera and the measurement paper. Thus, to avoid omitted variable bias, which could lead to the misinterpretation of the effects of one variable as those of another, it is crucial to include resolution as a variable in the model. Furthermore, the varying coefficients demonstrate the advantages of using higher-resolution images for trichome detection in computer vision applications. The results show that increased resolution leads to improved detection accuracy, highlighting the importance of holding the measurement paper close to the camera and using a high-resolution image sensor for such tasks.

TABLE III
INTERACTION WHEN STRATIFIED BASED ON RESOLUTION

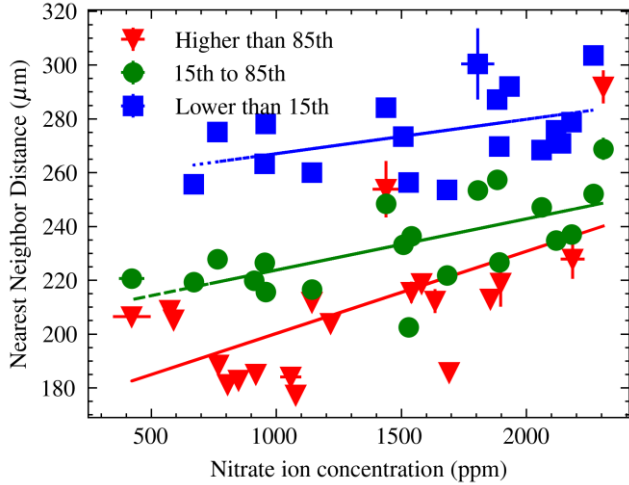| Percentile	Resolution (pixel)	Equation
Higher than 85th	$> 1.08 \times 10^6$	$y = 3.06 \times 10^{-2}x + 170$
15th to 85th	$1.08 \times 10^6 - 5.56 \times 10^5$	$y = 1.90 \times 10^{-2}x + 205$
Lower than 15th	$< 5.56 \times 10^5$	$y = 1.28 \times 10^{-2}x + 254$

FIGURE 15.Effect of resolution on the relationship between trichome density and nitrate concentration in leaves.

Table 4 displays the VIF values for all variables except for ISO speed ratings. After excluding ISO speed ratings, no variables with a VIF exceeding 10 were identified, indicating that multicollinearity was no longer a concern. To improve the interpretability of the model, ISO speed ratings were excluded as a variable in subsequent analyses due to their strong correlation with other variables and their potential to obscure the individual effects of each predictor. Instead, the modeling process included variables such as nearest neighbor distance, resolution, and exposure time, which were deemed to have a more independent impact on the response variable.

TABLE IV
VIF VALUE AFTER DIMENSIONALITY REDUCTION

Feature	VIF
Nearest Neighbor Distance	8.63
Resolution	6.49
Exposure Time	3.10

D. Performance of the Proposed Method

Figure 16 shows the learning curve of the LightGBM model over 100 boosting rounds with default settings, showing a gradual increase in the AUC-PR values for the training sets after each boosting round. This improvement indicates that the model has been adequately trained.
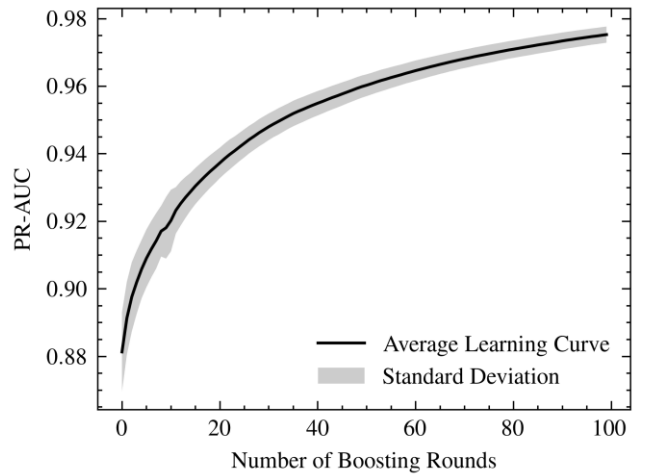

FIGURE 16.Learning curve of the LightGBM model.

Table 5 shows the predictive performance of the classification model at the different nitrate concentration thresholds. Regarding the trade-off between precision and recall, the model achieves highly balanced values.

TABLE V
PREDICTIVE PERFORMANCE IN TERMS OF THE NEED FOR ADDITIONAL FERTILIZER USING LOOCV AT VARIOUS NITRATE ION (PPM) THRESHOLDS

Evaluation Metrics	1600	1750	1900
Precision	0.68	0.76	0.79
Recall	0.66	0.76	0.79
F1 score	0.67	0.76	0.79
PR AUC	0.76	0.84	0.87
ROC AUC	0.64	0.68	0.58

For subsequent analyses, we defined a representative scenario using a nitrate concentration threshold of 1,783 ppm and 25 images captured from a single compound leaf. Using this representative scenario, predictions were made, allowing for an accurate assessment of the need for additional fertilization.

The predictive performance, as evaluated by the mPR, is 0.824, despite variations in the measurement data caused by differences in optical conditions. Figure 17(a) shows a

confusion matrix depicting true positives, false positives, true negatives, and false negatives. The predictions do not show substantial bias toward false positives or false negatives, indicating a balanced performance in identifying both classes correctly. This lack of bias is also evident from the balanced results presented in Table 5, which includes the F1 score, AUC-PR, and AUC-ROC values, as well as the PR curve in Figure 17(b) and the ROC curve in Figure 17(c).
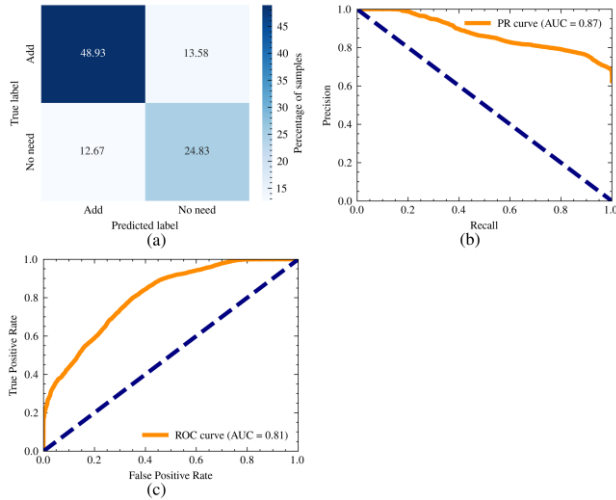

FIGURE 17. Performance of the model during LOOCV in a representative setting. (a) Confusion matrix for classification outcomes; (b) precision–recall (PR) curve analysis; (c) receiver operating characteristic (ROC) curve analysis.

Figure 18 illustrates the relationship between the number of input images and the model's predictive performance. Using a single image yields a mean AUC-PR (mPR) of 0.799 and increasing the number of input images leads to better predictive performance.
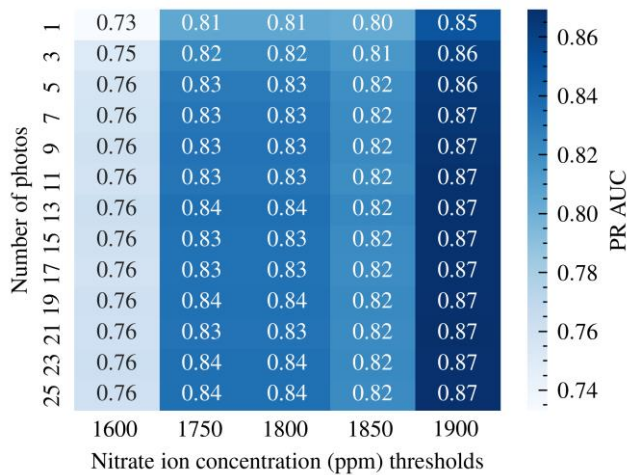
FIGURE 18. Model prediction performance by setting various thresholds and numbers of images.

Figure 19 shows the importance of the input variables on the model. Notably, the NND emerges as the variable with the highest importance, clearly indicating its substantial impact on th
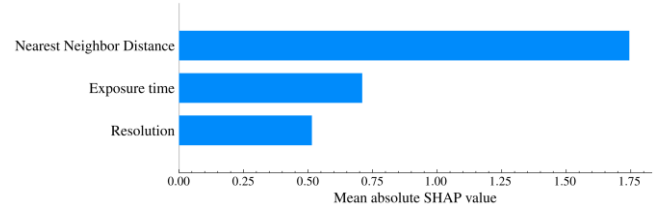
FIGURE 19. Variable importance during LOOCV with a representative model setting.

V. DISCUSSION

Tomatoes pose a challenge regarding detecting fertilizer stress through noncontact optical measurements of young leaf chlorophyll. This challenge arises from the nonlinear relationship between optical measurements and leaf nitrogen content, which distinguishes tomatoes from other crops [7], [11]. To address this problem, our study focused on trichomes, which are densely packed hair-like structures on leaf surfaces that have been less explored in previous research. We investigated the feasibility of detecting fertilizer stress by developing a device that utilizes trichome density as a primary predictor. These findings suggest the possibility of overcoming the limitations of conventional noncontact optical methods in assessing tomato fertilizer conditions. Our approach opens up new avenues for developing diagnostic devices that consider leaf surface structure.

However, it is essential to acknowledge that the diagnostic kits developed in this study have some limitations regarding their performance. We validated the performance of the kit through experiments using a well-designed setup that simulated different levels of fertilizer stress commonly found in agricultural production conditions. In addition, the tomato cultivation method used in the study involved cost-effective hydroponic cultivation using plastic buckets. The yields achieved were comparable to those obtained in commercial cultivation. This finding suggests that the cultivation method employed in this study closely simulated agricultural production conditions. However, it is uncertain whether all farmers will be able to establish optimal growing conditions for tomatoes to achieve higher yields, considering the financial costs involved in acquiring the necessary equipment. Consequently, there is a possibility of encountering environmental stresses beyond fertilizer stress, which could decrease the predictive performance of our novel method under these circumstances.

Traditionally, farmers have relied on visual inspection of leaf color, size, texture and overall plant health to assess the nutrient status of plants. However, the accuracy of this method is highly dependent on the farmers' experience and motivation, resulting in considerable variations among individuals. Consequently, standardizing the assessment of nutrient status becomes problematic, making it difficult to compare and evaluate the effectiveness of different approaches. The absence of standardization in nutrient status assessment hinders the highly advanced evaluation of the usefulness of diagnostic kits for a certain farmer solely based

on a comparison of their predictive accuracy. Thus, further demonstrations and validations employing more lagging indicators, such as financial metrics, are necessary to assess the practical applicability of these diagnostic kits in real-world agricultural settings.

Although various nutrient diagnostic kits are commercially available for assessing plant nutrient status, their high cost and potential difficulties in application to delicate plant tissues, such as young tomato leaves, limit their widespread adoption in practical farming settings. To overcome these challenges, we propose a novel, simple, and cost-effective method for assessing nutrient status in tomato plants, with a specific focus on young leaves, which are typically more sensitive to nutrient deficiencies and play a crucial role in plant growth and development. In addition to tomatoes, various plant species, including agriculturally important crops such as watermelon (*Citrullus lanatus*), eggplant (*Solanum melongena*), tobacco (*Nicotiana tabacum*), soybean (*Glycine max*), and cannabis (*Cannabis sativa*), are known to have abundant trichomes. The proposed trichome-based method for assessing nutrient status has the potential to be applied to other plant species that have dense trichomes near their growing points, expanding the scope of this novel approach and potentially improving real-time nutrient management practices in a wide range of crops, thereby enhancing the efficiency and precision of fertilizer application. By optimizing fertilizer application and reducing waste, this method could lead to increased crop yields, lower production costs, and reduced environmental impact, ultimately contributing to more sustainable agricultural practices. Further research is needed to validate the effectiveness of this method in various crop species and investigate the potential integration of this approach with other precision agriculture technologies, such as remote sensing, for more comprehensive and efficient nutrient management strategies.

VI. CONCLUSION

This study focused on developing a novel method for detecting fertilizer stress in tomato plants by measuring the density of trichomes on their leaves. The study also encompassed setting up and evaluating the experimental environment necessary for conducting these assessments. The developed diagnostic kit enables noncontact detection of fertilizer stress in plants, obviating the need for customized sensing device design and permitting the use of a universal diagnostic kit at a lower cost than that of traditional devices while accurately assessing the nutrient status of tomato plants. The findings of this study present a novel approach for designing diagnostic devices for detecting fertilizer stress in plants by considering the structure of the plant surface.

REFERENCES

[1] C.Sonneveld, J.Van den Ende, and S.De Bes, "Estimating the chemical compositions of soil solutions by obtaining saturation extracts or specific 1:2 by volume extracts", Plant and Soil, vol. 122, pp. 169-175, Mar. 1990. Accessed on: Apr. 17, 2024, DOI: 10.1007/BF02851971, [Online].

[2] Y.Chen et al., "Crop management based on multi-split topdressing enhances grain yield and nitrogen use efficiency in irrigated rice in China", Field Crops Research, vol. 184, pp. 50-57, Dec. 2015. Accessed on: Apr. 17, 2024, DOI: 10.1016/j.fcr.2015.09.006, [Online].

[3] G.Hochmuth, "Efficiency Ranges for Nitrate-Nitrogen and Potassium for Vegetable Petiole Sap Quick Tests", HortTechnology, vol. 4, pp. 218-222, Jul. 1994. Accessed on: Apr. 17, 2024, DOI: 10.21273/HORTTECH.4.3.218, [Online].

[4] P.Andersen et al., "Relationships of Nitrogenous Compounds in Petiole Sap of Tomato to Nitrogen Fertilization and the Value of these Compounds as a Predictor of Yield", HortScience, vol. 34, pp. 254-258, Apr. 1999. Accessed on: Apr. 17, 2024, DOI: 10.21273/HORTSCI.34.2.254, [Online].

[5] K.Wakamori and H.Mineno, "Optical Flow-Based Analysis of the Relationships between Leaf Wilting and Stem Diameter Variations in Tomato Plants", Plant Phenomics, vol. 2019, Jan. 2019. Accessed on: Apr. 17, 2024, DOI: 10.34133/2019/9136298, [Online].

[6] B.Klepper, V.Browning, and H.Taylor, "Stem Diameter in Relation to Plant Water Status", Plant Physiology, vol. 48, pp. 683-685, Dec. 1971. Accessed on: Apr. 17, 2024, DOI: 10.1104/pp.48.6.683, [Online].

[7] F.Padilla et al., "Proximal Optical Sensors for Nitrogen Management of Vegetable Crops: A Review", Sensors, vol. 18, pp. 2083, Jun. 2018. Accessed on: Apr. 17, 2024, DOI: 10.3390/s18072083, [Online].

[8] S.Locascio et al., "Nitrogen and Potassium Application Scheduling Effects on Drip-irrigated Tomato Yield and Leaf Tissue Analysis", HortScience, vol. 32, pp. 230-235, Apr. 1997. Accessed on: Apr. 17, 2024, DOI: 10.21273/HORTSCI.32.2.230, [Online].

[9] R.Coltman, "Yields of Greenhouse Tomatoes Managed to Maintain Specific Petiole Sap Nitrate Levels", HortScience, vol. 23, pp. 148-151, Feb. 1988. Accessed on: Apr. 17, 2024, DOI: 10.21273/HORTSCI.23.1.148, [Online].

[10] D.dela Torre, J.Gao, and C.Macinnis-Ng, "Remote sensing-based estimation of rice yields using various models: A critical review", Geo-spatial Information Science, vol. 24, pp. 580-603, Oct. 2021. Accessed on: Apr. 17, 2024, DOI: 10.1080/10095020.2021.1936656, [Online].

[11] G.Gianquinto et al., "A methodological approach for defining spectral indices for assessing tomato nitrogen status and yield", European Journal of Agronomy, vol. 35, pp. 135-143, Oct. 2011. Accessed on: Apr. 17, 2024, DOI: 10.1016/j.eja.2011.05.005, [Online].

[12] F.Padilla et al., "Threshold values of canopy reflectance indices and chlorophyll meter readings for optimal nitrogen nutrition of tomato", Annals of Applied Biology, vol. 166, pp. 271-285, Mar. 2015. Accessed on: Apr. 17, 2024, DOI: 10.1111/aab.12181, [Online].

[13] A.Cartelat et al., "Optically assessed contents of leaf polyphenolics and chlorophyll as indicators of nitrogen deficiency in wheat (Triticum aestivum L.)", Field Crops Research, vol. 91, pp. 35-49, Jan. 2005. Accessed on: Apr. 17, 2024, DOI: 10.1016/j.fcr.2004.05.002, [Online].

[14] F.Padilla et al., "Monitoring nitrogen status of vegetable crops and soils for optimal nitrogen management", Agricultural Water Management, vol. 241, pp. 106356, Nov. 2020. Accessed on: Apr. 17, 2024, DOI: 10.1016/j.agwat.2020.106356, [Online].

[15] H.Johnson, "Plant pubescence: An ecological perspective", The Botanical Review, vol. 41, pp. 233-258, Jul. 1975. Accessed on: Apr. 17, 2024, DOI: 10.1007/BF02860838, [Online].

[16] S.Kinoshita and S.Yoshioka, "Structural Colors in Nature: The Role of Regularity and Irregularity in the Structure", ChemPhysChem, vol. 6, pp. 1442-1459, Aug. 2005. Accessed on: Apr. 17, 2024, DOI: 10.1002/cphc.200500007, [Online].

[17] R.Middleton et al., "Self-assembled, disordered structural color from fruit wax bloom", Science Advances, vol. 10, Feb. 2024. Accessed on: Apr. 17, 2024, DOI: 10.1126/sciadv.adk4219, [Online].

[18] K.Thomas et al., "Function of blue iridescence in tropical understorey plants", Journal of The Royal Society Interface, vol. 7, pp. 1699-1707, Dec. 2010. Accessed on: Apr. 17, 2024, DOI: 10.1098/rsif.2010.0201, [Online].

[19] J.Barbour, R.Farrar, and G.Kennedy, "Interaction of fertilizer regime with host‐plant resistance in tomato", Entomologia Experimentalis et Applicata, vol. 60, pp. 289-300, Sep. 1991. Accessed on: Apr. 17, 2024, DOI: 10.1111/j.1570-7458.1991.tb01549.x, [Online].

[20] E.Hoffland, "Nitrogen Availability and Defense of Tomato Against Two-spotted Spider Mite", Journal of Chemical Ecology, vol. 26, pp. 2697-2711, Dec. 2000. Accessed on: Apr. 17, 2024, DOI: 10.1023/A:1026477423988, [Online].

[21] R.Wilkens et al., "Resource availability and the trichome defenses of tomato plants", Oecologia, vol. 106, pp. 181-191, Apr. 1996. Accessed on: Apr. 17, 2024, DOI: 10.1007/BF00328597, [Online].

[22] N.Bergau et al., "The development of type VI glandular trichomes in the cultivated tomato Solanum lycopersicum and a related wild species S. habrochaites", BMC Plant Biology, vol. 15, pp. 289, Dec. 2015. Accessed on: Apr. 17, 2024, DOI: 10.1186/s12870-015-0678-z, [Online].

[23] Q. Li et al. (2014, Jul.). The effects of nitrogen on micro-structure of tomato leaf. presented at 2014 ASABE Annual International Meeting. [Online]. Available: DOI 10.13031/aim.20141912263

[24] G.Leite et al., "Effect of fertilization levels, age and canopy height of Lycopersicon hirsutum on the resistance to Myzus persicae", Entomologia Experimentalis et Applicata, vol. 91, pp. 267-273, May. 1999. Accessed on: Apr. 17, 2024, DOI: 10.1046/j.1570-7458.1999.00493.x, [Online].

[25] Z.Zhao et al., "Object Detection With Deep Learning: A Review", IEEE Transactions on Neural Networks and Learning Systems, vol. 30, pp. 3212-3232, Nov. 2019. Accessed on: Apr. 17, 2024, DOI: 10.1109/TNNLS.2018.2876865, [Online].

[26] L.Vincent and P.Soille, "Watersheds in digital spaces: an efficient algorithm based on immersion simulations", IEEE Transactions on Pattern Analysis and Machine Intelligence, vol. 13, pp. 583-598, Jun. 1991. Accessed on: Apr. 17, 2024, DOI: 10.1109/34.87344, [Online].

[27] J.Mendes et al., "Smartphone Applications Targeting Precision Agriculture Practices—A Systematic Review", Agronomy, vol. 10, pp. 855, May. 2020. Accessed on: Apr. 17, 2024, DOI: 10.3390/agronomy10060855, [Online].

[28] Z.Li et al., "Non-invasive plant disease diagnostics enabled by smartphone-based fingerprinting of leaf volatiles", Nature Plants, vol. 5, pp. 856-866, Aug. 2019. Accessed on: Apr. 17, 2024, DOI: 10.1038/s41477-019-0476-y, [Online].

[29] M.Neumann et al., "Erosion Band Features for Cell Phone Image Based Plant Disease Classification", 2014 22nd International Conference on Pattern Recognition, pp. 3315-3320, Aug. 2014. Accessed on: Apr. 17, 2024, DOI: 10.1109/ICPR.2014.571, [Online].

[30] A.Johannes et al., "Automatic plant disease diagnosis using mobile capture devices, applied on a wheat use case", Computers and Electronics in Agriculture, vol. 138, pp. 200-209, Jun. 2017. Accessed on: Apr. 17, 2024, DOI: 10.1016/j.compag.2017.04.013, [Online].

[31] A.Elhassouny and F.Smarandache, "Smart mobile application to recognize tomato leaf diseases using Convolutional Neural Networks", 2019 International Conference of Computer Science and Renewable Energies (ICCSRE), pp. 1-4, Jul. 2019. Accessed on: Apr. 17, 2024, DOI: 10.1109/ICCSRE.2019.8807737, [Online].

[32] J.Münch et al. (2013, Dec.). Creating Minimum Viable Products in Industry-Academia Collaborations. presented at Lean Enterprise Software and Systems. [Online]. Available: DOI 10.1007/978-3-642-44930-7_9

[33] Intel Corporation and Willow Garage Inc. , "opencv-contrib-python", Version 4.6.0.66, [Online]. Available: https://github.com/opencv/opencv_contrib. Accessed on: Apr. 17, 2024.

[34] J.Seibert, J.Boone, and K.Lindfors, "Flat-field correction technique for digital detectors", SPIE Proceedings, vol. 3336, pp. 348-354, Jul. 1998. Accessed on: Apr. 17, 2024, DOI: 10.1117/12.317034, [Online].

[35] J.Glas et al., "Plant Glandular Trichomes as Targets for Breeding or Engineering of Resistance to Herbivores", International Journal of Molecular Sciences, vol. 13, pp. 17077-17103, Nov. 2012. Accessed on: Apr. 17, 2024, DOI: 10.3390/ijms131217077, [Online].

[36] P.Clark and F.Evans, "Distance to Nearest Neighbor as a Measure of Spatial Relationships in Populations", Ecology, vol. 35, pp. 445-453, Oct. 1954. Accessed on: Apr. 17, 2024, DOI: 10.2307/1931034, [Online].

[37] P.Cunningham and S.Delany, "k-Nearest Neighbour Classifiers - A Tutorial", ACM Computing Surveys, vol. 54, pp. 1-25, Jul. 2022. Accessed on: Apr. 17, 2024, DOI: 10.1145/3459665, [Online].

[38] D. Cournapeau, "scikit-learn", Version 1.2.1, [Online]. Available: https://github.com/scikit-learn/scikit-learn. Accessed on: Apr. 17, 2024.

[39] The Water-Culture Method for Growing Plants Without Soil, Dennis R. Hoagland and Daniel I. Arnon, eds., Berkeley, CA, USA: University of California, College of Agriculture, Agricultural Experiment Station, 1950. [Online]. Available: https://archive.org/details/watercultureme3450hoag

[40] R.Velazquez-Gonzalez et al., "A Review on Hydroponics and the Technologies Associated for Medium- and Small-Scale Operations", Agriculture, vol. 12, pp. 646, Mar. 2022. Accessed on: Apr. 17, 2024, DOI: 10.3390/agriculture12050646, [Online].

[41] Y.Ishihara, H.Hitomi, and Y.Yamaki, "Effect of Composition of an Improved Nutrient Solution for a Closed Hydroponic System on Nutrient Absorption by Tomatoes", Horticultural Research (Japan), vol. 6, pp. 391-397, Jul. 2007. Accessed on: Apr. 17, 2024, DOI: 10.2503/hrj.6.391, [Online].

[42] Docker, Inc. , "Docker", [Online]. Available: https://www.docker.com. Accessed on: Apr. 17, 2024.

[43] Python Software Foundation, "Python", Version 3.10.9.final.0, [Online]. Available: https://www.python.org. Accessed on: Apr. 17, 2024.

[44] Project Jupyter, "datascience-notebook", Docker image, Version cde8b4389ade, [Online]. Available: https://hub. docker.com/r/jupyter/datascience-notebook. Accessed on: Apr. 17, 2024.

[45] scikit-learn-contrib, "imbalanced-learn", Version 0.12.0, [Online]. Available: https://github.com/scikit-learn-contrib/imbalanced-learn. Accessed on: Apr. 17, 2024.

[46] K.Guolin and Microsoft Research, "LightGBM", Version 3.3.5, [Online]. Available: https://github.com/microsoft/LightGBM. Accessed on: Apr. 17, 2024.

[47] S.Lundberg, S. Lee, "SHAP", Version 0.43.0, [Online]. Available: https://github.com/slundberg/shap. Accessed on: Apr. 17, 2024.

[48] S.Ianaré, "ExifRead", Version 3.0.0, [Online]. Available: https://github.com/ianare/exif-py. Accessed on: Apr. 17, 2024.

[49] A.Zuur, E.Ieno, and C.Elphick, "A protocol for data exploration to avoid common statistical problems", Methods in Ecology and Evolution, vol. 1, pp. 3-14, Mar. 2010. Accessed on: Apr. 17, 2024, DOI: 10.1111/j.2041-210X.2009.00001.x, [Online].

[50] G.Haixiang et al., "Learning from class-imbalanced data: Review of methods and applications", Expert Systems with Applications, vol. 73, pp. 220-239, May. 2017. Accessed on: Apr. 17, 2024, DOI: 10.1016/j.eswa.2016.12.035, [Online].

[51] N.V.Chawla et al., "SMOTE: Synthetic Minority Over-sampling Technique", Journal of Artificial Intelligence Research, vol. 16, pp. 321-357, Jun. 2002. Accessed on: Apr. 17, 2024, DOI: 10.1613/jair.953, [Online].

[52] K.Guolin et al., "LightGBM: a highly efficient gradient boosting decision tree", Proceedings of the 31st International Conference on Neural Information Processing Systems, pp. 3149-3157, 2017.

[53] M.Hossin, M.N.Sulaiman, "A Review on Evaluation Metrics for Data Classification Evaluations", International Journal of Data Mining & Knowledge Management Process, vol. 5, pp. 01-11, Mar. 2015. Accessed on: Apr. 17, 2024, DOI: 10.5121/ijdkp.2015.5201, [Online].

[54] L.Jeni, J.Cohn, and F.De La Torre, "Facing Imbalanced Data--Recommendations for the Use of Performance Metrics", 2013 Humaine Association Conference on Affective Computing and Intelligent Interaction, pp. 245-251, Sep. 2013. Accessed on: Apr. 17, 2024, DOI: 10.1109/ACII.2013.47, [Online].

[55] S.Lundberg, S.Lee, "A Unified Approach to Interpreting Model Predictions", Proceedings of the 31st International Conference on Neural Information Processing Systems, pp. 4768-4777, 2017.

[56] F.Maureira, K.Rajagopalan, and C.Stöckle, "Evaluating tomato production in open-field and high-tech greenhouse systems", Journal of Cleaner Production, vol. 337, pp. 130459, Feb. 2022. Accessed on: Apr. 17, 2024, DOI: 10.1016/j.jclepro.2022.130459, [Online].